Structural Monitoring and Maintenance, *Vol. 12, No. 2 (2025) 137-159*
https://doi.org/10.12989/smm.2025.12.2.137

A comparative study on ultrasonic immersion and laser-vibrometer tests for characterization of cement based materials

Sabah H.L. Fartosy[1a], Edward Ginzel[2], Giovanni Cascante[2b] and Ahmet S. Kırlangıç*[3]

[1]*College of Engineering, Mustansiriyah University, Baghdad, Iraq*
[2]*Department of Civil Engineering, University of Waterloo, Waterloo, ON N2L 3G1, Canada*
[3]*School of Computing, Engineering, and Digital Technologies, Teesside University, Middlesbrough TS1 3PX, United Kingdom*

(*Received October 15, 2024, Revised January 8, 2025, Accepted March 19, 2025*)

Abstract. Concrete's heterogeneous structure makes it a highly dispersive medium for wave propagation, affecting ultrasonic test measurements. Aggregate grain size is a major source of heterogeneity, influencing wave characteristics. To have a clear understand of the effect of grain size on wave properties, it is essential to eliminate variability from aggregate-mortar interface and concrete mixture design; this requires examining specimens made of identical aggregates. Coupling also influences wave measurements significantly. While ultrasonic immersion testing provides consistent coupling, it isn't suitable for in-situ testing. Laser vibrometers (LV) have the potential to offer a reliable non-contact alternative for in-situ measurements. This study investigates the influences of aggregate content and coupling on ultrasonic measurements. Immersion and LV tests are performed on homogeneous (acrylic, nylon) and heterogeneous (concrete, mortar with varying glass bead content) specimens. Material properties, including wave velocities, acoustic impedance, elastic moduli, and attenuation, are determined using both methods. Wave signals are analyzed in time and frequency domains to identify optimal material characterization method. Results indicate that attenuation primarily originates from the irregular shape of aggregates compared to the smooth surface of glass beads. Furthermore, LV measurements of P-wave velocity and attenuation strongly agree with immersion tests, suggesting LV as a viable alternative.

Keywords: aggerate grain size; cementitious materials; laser vibrometer; mechanical properties; NDT; ultrasonic immersion test

1. Introduction

Non-destructive tests based on ultrasonic stress waves are commonly used for characterization and condition assessment of cement-based materials. An extensive body of literature exists, investigating multiple stress wave characteristics, such as velocity, attenuation, dispersion, to determine which can be used as diagnostic parameters for purposes such as strength measurement, defect/damage detection, crack depth estimation, and concrete's impedance monitoring (Wiciak *et*

*Corresponding author, Ph.D., E-mail: s.kirlangic@tees.ac.uk
[a]Ph.D.
[b]Professor

http://www.techno-press.org/?journal=smm&subpage=7 ISSN: 2288-6605 (Print), 2288-6613 (Online)

al. 2020, Yang *et al*. 2009, Gucunski *et al*. 2015, Kirlangic and Iscan 2022, Shiotani *et al.* 2024, Pham *et al*. 2022, Ta *et al*. 2024). Primary (P-wave) and shear (S-wave) wave velocities are two major wave characteristics that are essential in practical applications. These velocities are measured to identify primarily the mechanical properties of concrete, e.g. Young's modulus and shear modulus (ASTM C597-22, ASTM C1383-23). The straightforward test configuration and directness of calculations make the wave velocities the most sought-after wave parameters to measure. Attenuation and dispersion are also heavily exploited wave characteristics, preferred mainly for assessing the condition of concrete (Aggelis *et al*. 2009, Lin *et al*. 2020, Kirlangic *et al*. 2020). However, measuring these latter two typically requires either multiple sensors or advanced signal processing, limiting their commercial use.

Concrete is inherently a highly heterogenous material, primarily composed of cement, aggregates, water, and air voids. Aggregate gradation, aggregate-mortar interface, micro-cracks and other defects, make concrete a highly dispersive medium for wave propagation, affecting the wave characteristics (Ju *et al.* 1999, Chaix *et al*. 2006, Tarek and Mahmood 2016, Gosálbez *et al*. 2018, Hasannejad *et al*. 2022). Since P-wave and S-wave velocities are typically measured based on the arrival time of the wavefront (ASTM C1383-23), the effect of heterogeneity on the measurements is relatively limited. In contrast, wave attenuation is directly influenced by the material's heterogeneity, which causes wave scattering and consequently complex attenuation behavior (Anugonda *et al*. 2001). Previously, aggregate grain size, a major source of heterogeneity, is reported to have a stronger impact on wave attenuation compared to pulse velocity based on a study conducted on mortar and concrete specimens (Philippidis and Aggelis 2005). To clearly understand the effect of aggregate grain size on wave properties, and hence the material properties of concrete, it is essential to conduct experimental studies on specimens made of identical aggregates with the same shape. This approach will eliminate the influence of the random nature of aggregate-mortar interface and differences in concrete mixture design on the ultrasonic measurements, isolating the sole effect of the heterogeneity caused by the amount of aggregates.

Accurate estimation of wave characteristics requires simple yet effective test techniques. One of the most widely used ultrasonic technique to determine material characteristics is the immersion test method. This test is applicable for the characterization of a wide variety of materials including polymers, metals, composites, and tissues (Selfridge 1985, Krautkrämer and Krautkrämer 2013, Ensminger and Bond 2011, O'Leary *et al*. 2002, Webster and Eren 2014, Buiochi *et al*. 2014, Bazylev and Lugovoi 2023). The immersion test can be performed either with a through-transmission configuration, in which a pair of transducers immersed in a water tank are aligned on a straight line, or with a pulse-echo setup configuration, where only a single transducer is deployed to both transmit and receive signals. Despite the simplicity of the pulse-echo configuration, the through-transmission configuration has advantages over the pulse-echo setup (Ginzel and Turnbull 2016). When testing highly attenuative material such as lossy, coarse-grained materials, the through-transmission configuration is favorable as there exists only one-way wave propagation path unlike the pulse-echo configuration which creates a two-way propagation path, causing higher attenuation and scattering losses. Another disadvantage that the pulse-echo configuration holds is that when the material's acoustic impedance closely matches the water's, the weaker signals are produced compared to the ones from the through-transmission approach. Furthermore, the only parameter needed from the through-transmission configuration is just the time offset between the transmitted and the received signals. The water used as coupling agent is the major advantage of this technique as it ensures high test-repeatability. P-wave and S-wave velocities, along with wave attenuation, can all be obtained from the immersion tests.

The through-transmission configuration has previously been utilized airborne to examine the effect of coarse aggregate content on wave attenuation (Kim *et al*. 1991, Gaydecki *et al*. 1992,

Otsuki *et al*. 2000). The testing procedure used in these studies is based on comparing a face-to-face reference waveform with the signals obtained from test specimens placed between transmitter and receiver transducers. The tested specimens included paste (cement and water), mortar (cement, sand, and water), and concrete (cement, sand, coarse aggregates, and water) with different water-cement ratios. In general, the results highlighted the significant influence of coarse aggregate content on the attenuation behavior, despite the concerns regarding the uncertainties in attenuation measurements caused by the inconstant coupling between specimens and transducers. Becker *et al*. (2003) utilized diffuse ultrasound technique to investigate the propagation of ultrasonic waves in cement-based specimens containing different sizes of glass beads as wave scatters. The results indicated that wave energy dissipation is dominated by the material attenuation rather than the losses occurring at the interface between cement paste and glass beads. Similarly, this study also raised concern regarding measurement uncertainties attributed to coupling variability.

This study aims to investigate the influence of heterogeneity due to the aggregate content in cementitious materials on ultrasonic test measurements while also addressing the impact of coupling on measurement accuracy. To achieve this dual objective, two distinct non-destructive testing (NDT) methods, namely immersion through transmission and laser vibrometer (LV), are utilized on two groups of specimens: homogenous (acrylic and nylon) and heterogeneous (concrete and mortar with 0%, 15%, 35%, and 50% glass beads) to determine their material properties, including P-wave and S-wave velocities, acoustic impedance, transmission and reflection coefficients, Young's and shear moduli, and attenuation coefficient. Furthermore, different signal parameters in both time and frequency domains are used to identify these properties to reveal which test method delivers consistent material characterization. The paper first reviews the background on mechanical waves, then explains the experimental campaign, and finally presents and discusses the tests results.

2. Background

In immersion test, the longitudinal bulk velocity V_l, also known as P-wave velocity, of a specimen is determined with respect to the travel time of the wave propagating in the water. This is compared with the arrival time of the wave signal measured after immersing the specimen into the water tank. Thus, the longitudinal bulk velocity is calculated as (Ginzel and Turnbull 2016)

$$V_l = \frac{V_w}{\frac{1+(t_s-t_w)V_w}{d}} \tag{1}$$

where V_w is the wave velocity in water at a certain temperature, t_w is the reference arrival time in water-tank without the specimen, t_s is the measured arrival time while the specimen is immersed, and d is the thickness of the specimen. For a given water temperature T_w (C°), the sound velocity in water V_w given in (Eq. (1)) is calculated using the Bilaniuk and Wong (1993) equation

$$V_w = 1402.39 + 5.04T_w - 0.058{T_w}^2 + 3.287 - 4{T_w}^3 - 0.56{T_w}^4 + 0.027{T_w}^5 \tag{2}$$

The shear wave (S-wave) velocity can also be determined by using the arrival times with and without the specimen immersed in the tank as (Ginzel and Turnbull 2016)

$$V_s = \frac{V_w}{\sqrt{sin^2(\theta_t)+\left[\frac{(t_s+t_w)V_w}{d}+cos^2(\theta_t)\right]^2}} \tag{3}$$

where θ_t is the incident angle determined by the goniometer rotation. Acoustic impedance Z is

another parameter that can be obtained from the immersion test. Having the P-wave velocity V_l determined as in (Eq. (1)), the impedance of the specimen being tested is calculated as

$$Z = \rho V_l \tag{4}$$

where is ρ is the specimen density. The determination of the acoustic impedances of water and specimen allows calculation of the coefficients of transmission T_c and reflection R_c at the interface between water and specimen. The coefficient representing the portion of the wave transmitted into the specimen is calculated as

$$T_c = \frac{4Z_1Z_2}{(Z_1+Z_2)^2} \tag{5}$$

Whereas the coefficient for the reflected wave is defined by

$$R_c = 1 - T_c \tag{6}$$

or

$$R_c = \left(\frac{(Z_2-Z_1)}{(Z_1+Z_2)}\right)^2 \tag{7}$$

Here Z_1 and Z_2 are the acoustic impedances of material 1 and material 2, in this case water and specimen, respectively.

Once the P-wave and S-wave velocities are obtained from the immersion test, the specimen's elastic constants, namely Poisson's ratio ν, Young's modulus E, and shear modulus G, can be determined using the following equations respectively

$$\upsilon = \frac{1-2\left(\frac{V_s}{V_l}\right)^2}{2-2\left(\frac{V_s}{V_l}\right)^2} \tag{8}$$

$$E = \frac{\rho V_l^2(1+\upsilon)(1-2\upsilon)}{(1-\upsilon)} \tag{9}$$

$$G = \rho V_s^2 \tag{10}$$

In addition to the material's elastic properties described above, wave attenuation, which is defined as the reduction in stress pressure, in this case the reduction in ultrasound intensity, can also be obtained from the immersion tests. Wave attenuation is particularly important compared to wave velocity for damage diagnosis in through-transmission technique because even a minor crack can cause significant reduction in acoustic impedance; whereas, a measurable change in wave velocity may not necessarily be observed (Berubé 2008). The attenuation is often expressed in decibels (dB) per unit length (Hellier 2001). It can also be defined in nepers (Np) per unit length. The reduction of one neper of the wave amplitude means its initial value has been reduced by 1/e, where e is the base of the natural logarithm.

A plane stress wave that attenuates as it propagates through a medium can be expressed as (Punurai 2006)

$$A(x,t) = A_o e^{-\alpha x} e^{i(\omega t - kx)} \tag{11}$$

where $A(x,t)$ is the wave amplitude at a distance x at a time t; A_o is the initial wave amplitude; ω is the angular frequency; k is the wave number (also known as the propagation factor); and α is

the attenuation coefficient. Isolating the exponential term that accounts for the decay in amplitude due to α, the following expression is obtained

$$A(x) = A_o e^{-\alpha x} \tag{12}$$

Taking the natural logarithm of each side of the expression given above yields to

$$\ln A(x) = \ln A_o - \alpha x \tag{13}$$

Thus, the attention in the propagating wave between two locations x_1 and x_2, where $x_1 < x_2$, can be defined as

$$\alpha = \frac{1}{x_2 - x_1} \ln \frac{A(x_1)}{A(x_2)} \tag{14}$$

Here, α is in Np/unit length. Given in logarithm with base 10, it can also be expressed in dB/unit length as

$$\alpha = \frac{1}{(x_2 - x_1)} 20\, log_{10} \frac{A(x_1)}{A(x_2)} \tag{15}$$

For a given distance or time, one decibel is 8.68 times the value in nepers. In practice, a variety of wave signal quantities can be studied to estimate the attenuation coefficient. For example, if the peak-to-peak amplitude in the time history of a wave signal is preferred, then α can be calculated as

$$\alpha = \frac{1}{d_s} 20\, log_{10} \frac{Pk_o(t)}{Pk_z(t)} \tag{16}$$

where Pk_o and Pk_z are the peak-to-peak wave amplitudes measured at two locations apart with a distance d_s in the medium. Eq. 16 can also be adapted to calculate the wave attenuation in frequency domain by examining either the maximum magnitude or the spectral area (*SA*) of the frequencies in interest (Kirlangic 2016).

3. Experimental works

The experimental work consists of two sets of tests including the ultrasonic immersion and laser-vibrometer tests as explained below in detail.

3.1 Immersion through-transmission test setup and procedure

The experimental setup developed by Ginzel and Turnbull (2016) is followed for the immersion test, which consists of a pulser-receiver (Adaptronics-PCPR100) utilized in conjunction with a data acquisition software (Winspect) and an immersion tank made of acrylic with a plastic base filled with distilled water. Two 500 kHz immersion type transducers (UTX-IX130) are deployed to emit and receive ultrasonic signals. The tank is equipped with a rotating specimen holder that can be used for obtaining shear wave signals (Fig. 1). During the ultrasonic tests, the pulser-receiver is used to generate a bi-polar ultrasonic pulse with a frequency of 650 kHz at a voltage of 250 volts. A 100MHz analogue to digital converter (STR8100) is used for the digitalization of the wave signals, which are first filtered using a built-in bandpass filter (0.1 MHz to 14 MHz).

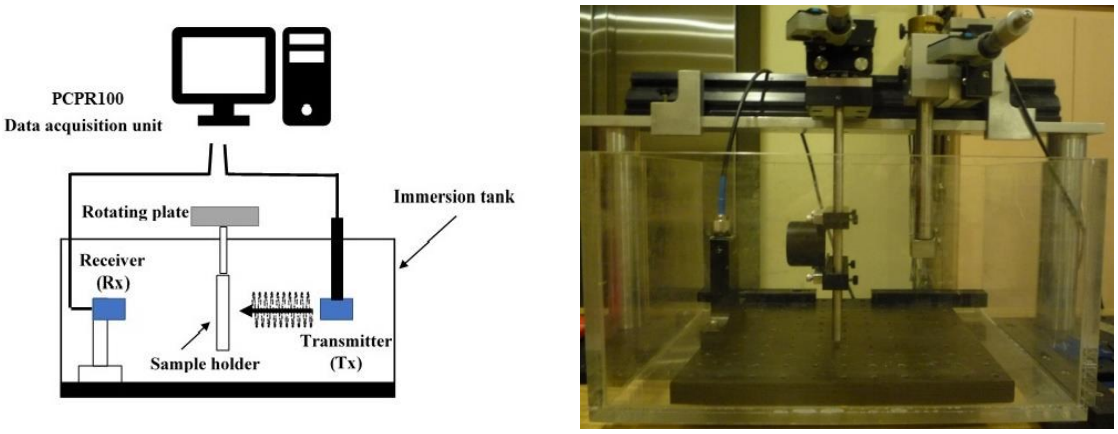

Fig. 1 (left) Immersion through-transmission test setup (adapted from Ginzel and Turnbull 2016), (right) immersion tank

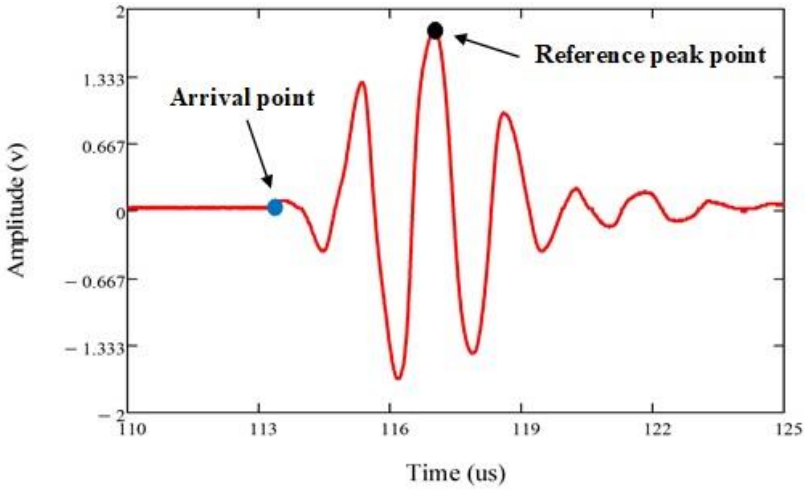

Fig. 2 Determination of the reference time points in the wave signal

In the immersion tests, the test specimen is placed perpendicular to the ultrasonic beam between the transmitter and receiver probes in order to capture the response. The first step during the test is to acquire a signal in the water-tank without any specimen to use it as a reference water path signal. Then, the temperature of the water is recorded to determine the wave velocity in the water. Fig. 2 displays a typical signal acquired in the water-tank with no specimen, where two reference points indicating the arrival time of the wave signal (arrival point) and the maximum amplitude at the peak cycle (peak point) are marked. Similarly, these two reference points are picked for the wave signal recorded whilst the specimen is placed in the tank to obtain the P-wave velocity.

An important advantage of the immersion setup is its ability to generate shear waves by rotating the goniometer (rotating base) to a critical rotation angle θ_t. In accordance with the Snell's

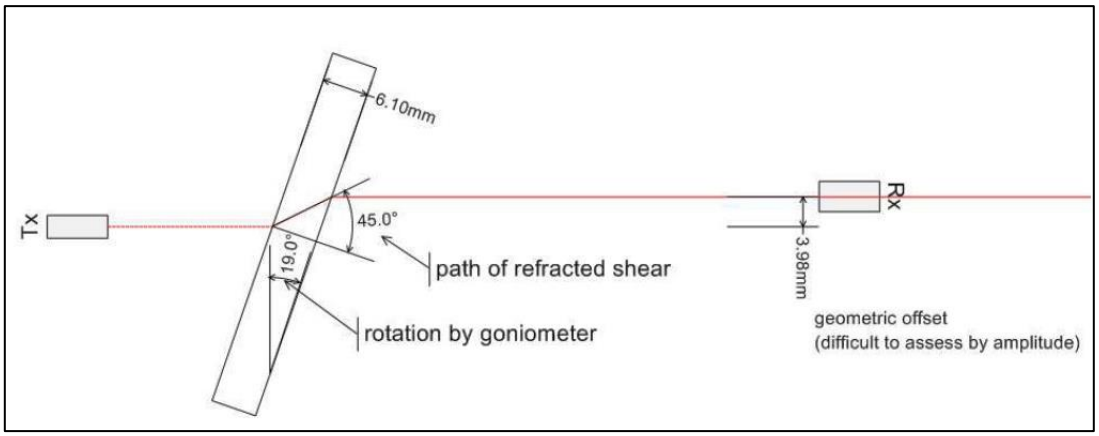

Fig. 3 Illustration of the S-wave velocity measurement in through-transmission immersion test setup (Ginzel and Turnbull 2016)

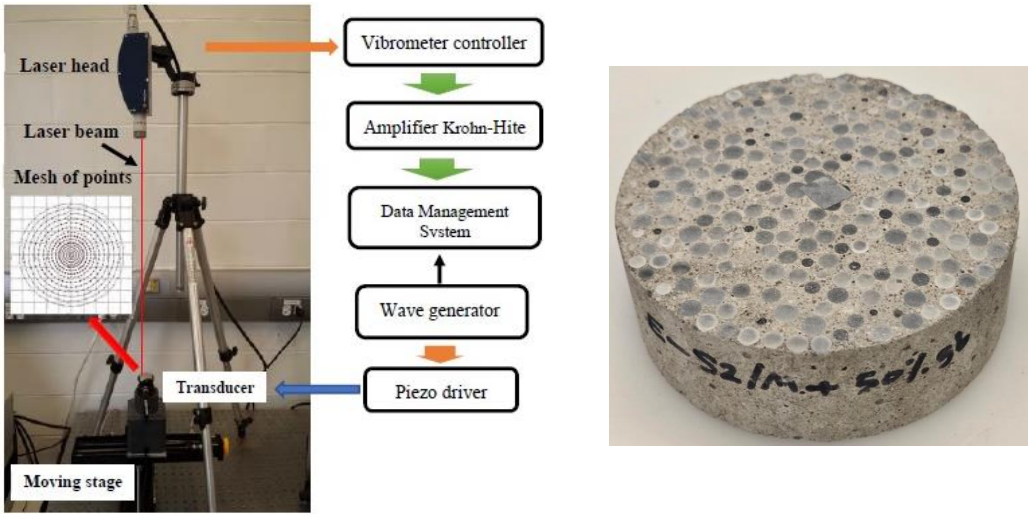

Fig. 4 (left) The laser vibrometer test setup, (right) a typical specimen

Table 1 The specimen mixtures

Name	Cement (kg)	Sand (kg)	Gravel (kg)	Glass beads (kg)	Proportions
Concrete (Cr)	0.8	1.2	1.6	NA	1:1.5:2:0
Mortar (Mr0%)	1.2	2.4	NA	NA	1:2:0:0
Mortar+15%gb (Mr15%)	1.00	2.0	NA	0.6	1:2:0:0.5
Mortar+35%gb (Mr35%)	1.00	1.2	NA	1.4	1:1:1.5
Mortar+50%gb (Mr50%)	1.00	0.6	NA	2.00	1:0.5:0:2

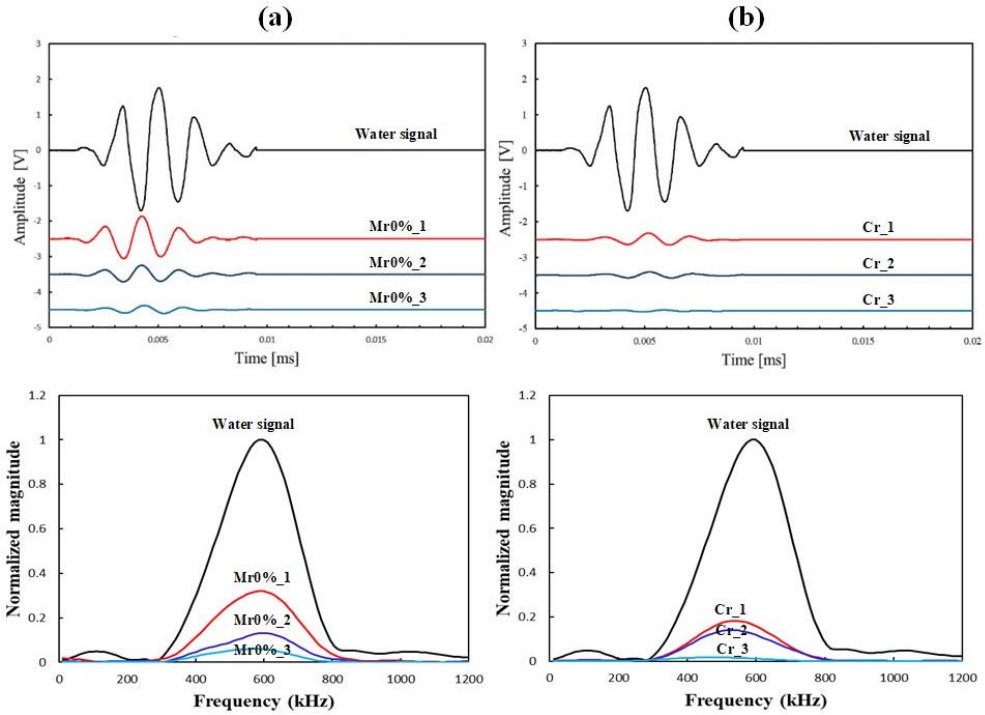

Fig. 5 Typical waveforms and corresponding frequency spectra of (a) mortar and (b) concrete specimens

law, at the critical angle, first, the longitudinal wave mode is totally internally reflected within the specimen letting only the shear wave mode propagate. As illustrated in Fig. 3, the shear mode exits the specimen from the far surface and converts back to longitudinal mode in the water. The critical rotation angle recorded during the test is then used to calculate the shear wave velocity V_S as given by Eq. (3).

3.2 Laser vibrometer test setup and procedure

A laser vibrometer, which consists of a laser head (Polytec OFV-534), vibrometer controller (Polytec OFV-2570), data management system, vibration isolated workstation, and high-resolution positioning controller, is utilized to examine the specimens (Polytec GmbH, 2013). The complete test setup also includes a wave generator (Keysight), an amplifier (Krohn-Hite), a piezo-driver, and one of the piezoelectric transducers used in the immersion tests. The transducer is placed on one side of the specimen being tested with the help of vacuum grease used as the coupling agent, and the laser head is aimed at the opposite side of the specimen as depicted in Fig. 4. The transducer is excited with a single cycle square-wave pulse generated by the function generator, with a nominal resonance frequency of 500 kHz and amplitude of 125 volts. The signals are recorded after being filtered by a high pass filter with a cut-off frequency at 1 kHz and amplified with a gain of 20 dB. To minimize random noise and enhance signal quality, 100 readings are averaged for each laser measurement. The averaged time history of the signal is then converted to a frequency spectrum using the fast Fourier transform (FFT).

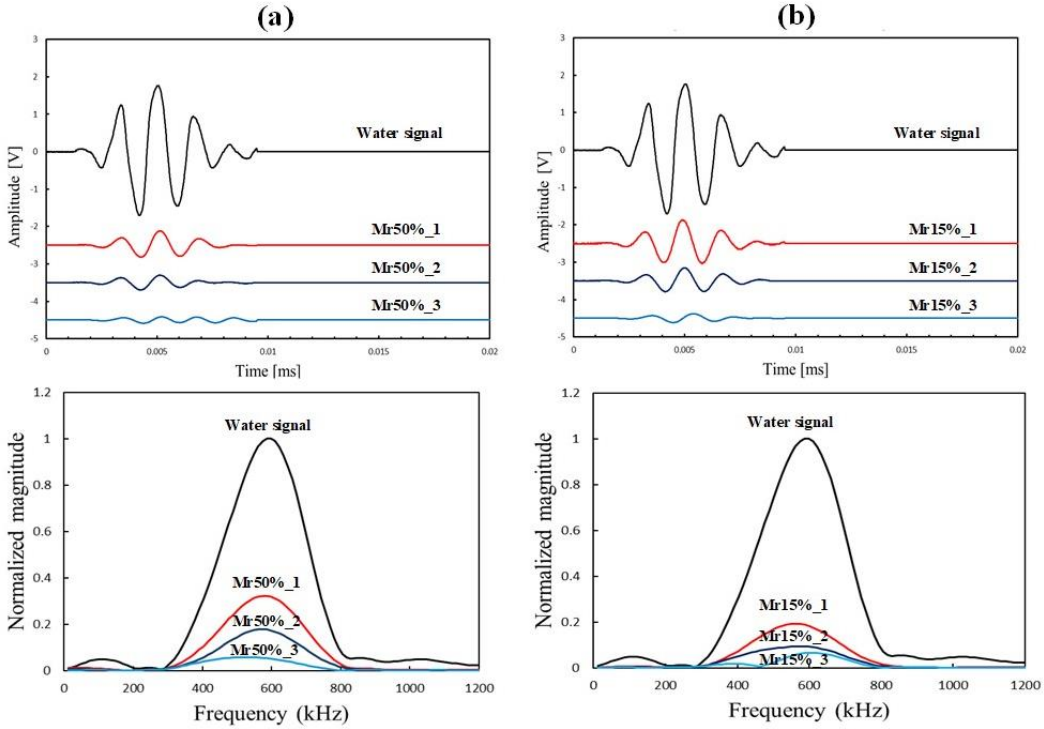

Fig. 6 Typical waveforms and corresponding frequency spectra for (a) Mr50% and (b) Mr15%

3.3 Specimen preparations

Five hardened cement-based cylindrical specimens (10 cm in diameter and 20 cm in height) are prepared with specific mixtures as shown in Table 1. These specimens include one concrete (made of cement, fine and coarse aggregates, and water) and four mortar (made of cement, sand, and water) specimens. Three of the mortar cylinders are mixed with borosilicate glass beads at different levels; 15%, 35%, and 50% by mass, while one mortar cylinder is kept without adding any beads. A typical specimen mixed with glass beads can be seen in Fig. 4. The weight fraction of glass beads is determined by dividing the glass weight by the specimen weight. The diameter of the glass beads, which is 6 mm, represents half of the nominal size of the coarse aggregates used in the mixture of the concrete specimens. All specimens are made of Portland type I cement with a water/cement mass ratio of 0.47, and are stored in a humidity room for 28 days of curing.

From each specimen, three discs (10 cm in diameter) with different thicknesses (2 cm, 4 cm, and 8 cm) are cut with a saw machine. The thicknesses of the discs are determined based on the approximate wavelength (λ=10 mm) of the pulse generated by the transducer, which are corresponding to 2λ, 4λ, and 8λ to avoid nearfield effects during the ultrasonic measurements. Two reference discs made of acrylic (11 cm in diameter and 2 cm in height) and nylon (11.5 cm in diameter and 2 cm in height) are employed for reference measurements as they are considered homogenous for the ultrasonic wavelength used in this study.

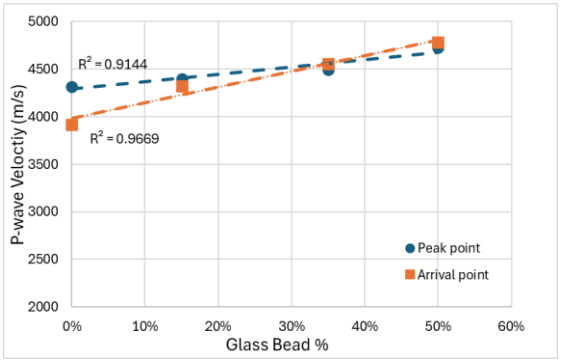

(a) Mean P-wave velocity

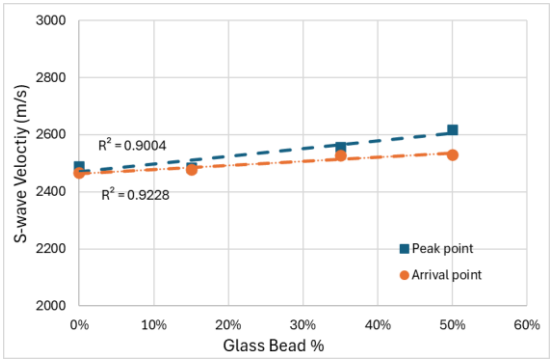

(b) Mean S-wave velocity

Fig. 7 Velocities with respect to glass bead %

4. Test results and discussions

4.1 Immersion test results

Immersion tests are conducted on a variety of cementitious specimens to investigate the effect of grain size on the wave parameters. The presence of coarse aggregates and glass beads increases the degree of heterogeneity, and therefore the interaction of the material structure with the propagating waves can be investigated by examining the wave signals obtained from these specimens. Comparison of the signals acquired from the water-tank without any specimen and homogenous materials, namely acrylic and nylon, with the ones from the cement-based specimens also set a reference baseline for non-heterogeneous conditions. The measured wave parameters, extracted from the recorded wave signals, including P-wave and S-wave velocities, acoustic impedance, transmission and reflection coefficients along with the elastic material properties such as Young's and shear moduli, and attenuation coefficient are tabulated in Table 2. These properties are calculated for the five types of specimens with three different thicknesses so that the effect of specimen thickness can also be examined along with the heterogeneity.

Typical waveforms obtained from the mortar and concrete specimens with three different thicknesses are displayed in Fig. 5. As a first observation, the wave signals obtained from the mortar samples present less attenuation consistently for all three thicknesses compared to the ones obtained from the concrete samples. This is expected given the fact that the maximum grain size in the mortar is 4.75 mm while it is 12 mm for the concrete, which causes a higher degree of heterogeneity in the concrete samples compared to the mortar ones. Similarly, as the percent of the glass beads increases in the mortar samples, the wave attenuation becomes more apparent due to higher quantity of larger grains as demonstrated in Fig. 6, where the waves propagating in the mortar samples containing 15% and 50% beads can be compared. Following these visual observations, further examinations are performed on the measured mechanical properties as presented next.

4.1.1 Wave velocities

The P-wave and S-wave velocities, given in Table 2, are calculated by using (Eqs. (1) and (3)) for two different reference time points; namely the first arrival point and peak point. In overall, the

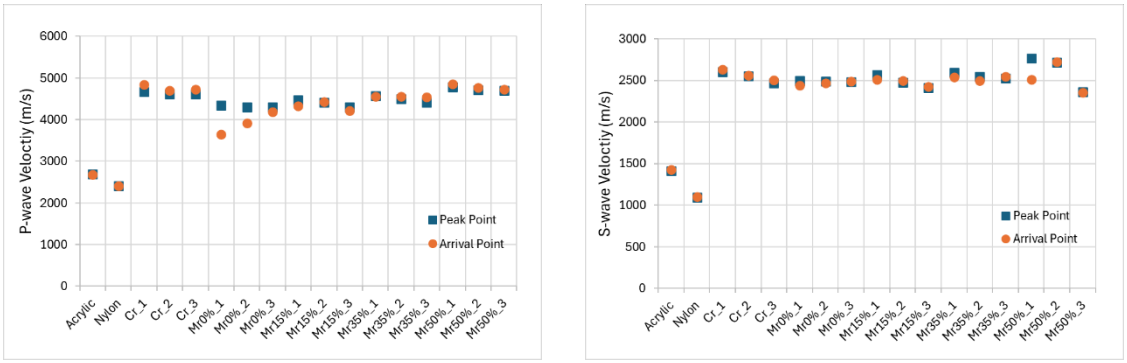

(a) P-wave velocity (b) S-wave velocity

Fig. 8 Velocities determined by two reference time point approaches, namely peak point and arrival point

cement-based specimens are found to have the P-wave and S-wave velocities at round 4500 m/s and 2650 m/s, respectively. Both velocities display an increasing trend with higher percent of the glass beads in the mortar. Particularly, for the most stiff specimens, namely Cr and Mr50%, the P-wave velocity is observed to be approximately 100 m/s higher compared to the other samples in accordance with the increased material stiffness due to the existence of aggregates and 50% glass beads. The stiffer structures of these specimens lead the waves to travel faster as expected. The effect of the glass beads on the wave velocities can also be clearly observed on the plots given in Fig. 7. The mean velocities of the P and S waves, averaged velocities of the same class of mortar specimens, increases linearly with increasing glass bead percent with the coefficients of determination (R^2) higher than 0.9.

Both reference point approaches deliver P-wave and S-wave velocities with negligible variations for the homogenous reference specimens, Acr and Nyl, indicating the interchangeability of the approaches (Fig. 8). Regarding the heterogeneous cement-based specimens, the velocities determined based on both reference points display very good agreement for the majority of the samples (Fig. 8); relatively high discrepancy is observed in P-wave velocity only for two mortar samples, and one mortar sample for S-wave velocity. This demonstrates that preferring the peak point, which can be conveniently identified on the recorded wave signal, as the reference point instead of the arrival point improves the practicability of the velocity calculations without compromising the accuracy.

Lastly, the P-wave and S-wave velocities, determined using the peak point approach, reveal a subtle yet consistent variation in relation to specimen thickness across all cement-based specimens. As depicted in Table 2, there is a slight decreasing trend in both velocities as the specimen thickness increases. This trend is considered to be related to faster travelling higher frequencies. As the travel path, in other words specimen length, increases, the higher frequencies attenuate, causing an additional delay in the first arrival time. Nevertheless, the impact of thickness is deemed insignificant compared to the effect of the additional stiffness induced by the presence of glass beads since the coefficients of variance (*CV*) of P-wave and S-wave velocities range between 0.3% and 1.6%; and 0.2% and 6.8%, respectively. Notably, this trend is not observed in the velocities determined based on the arrival time approach. This can be attributed to the fact that the precise selection of the arrival time in the recorded signal is more susceptible to error in contrast to the peak point approach, which is a more straightforward selection process.

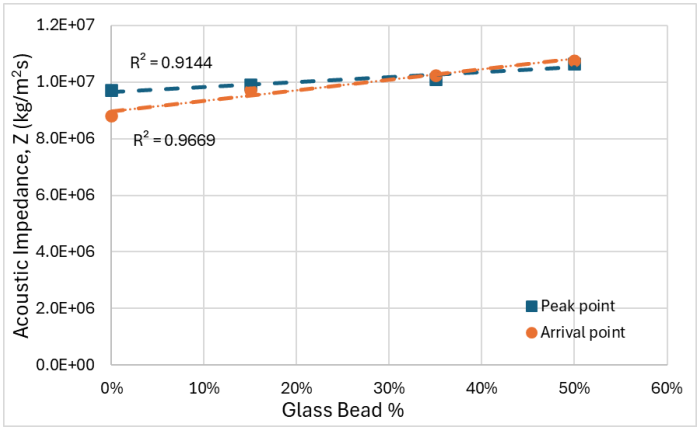

Fig. 9 Mean acoustic impedance with respect to glass bead %

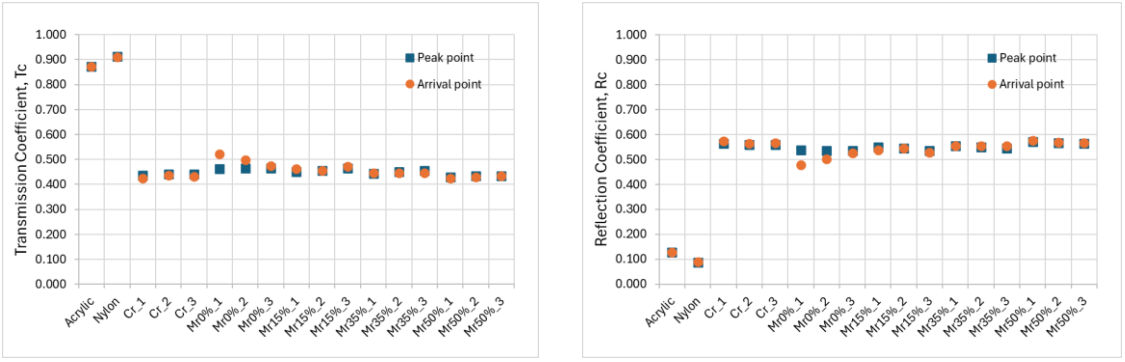

(a) P-wave velocity (b) S-wave velocity

Fig. 10 (a) Transmission and (b) reflection coefficients determined by two reference time point approaches, namely peak point and arrival point

4.1.2 Material acoustic parameters

Acoustic parameters, namely acoustic impedance (Z), transmission (T_c), and reflection (T_r) coefficients, are also determined with through-transmission immersion tests. Acoustic impedance plays an important role in the NDT applications for cement-based materials since it describes the relationship between the propagated waves and the material inherit structure. A mismatch in acoustic impedance between two materials such as concrete and air/water can be useful for the detection of any defect. The immersion test method in particular is a reliable procedure to determine the acoustic impedance of concrete materials thanks to its consistent coupling provided by the water-tank. Herein, the acoustic impedances of the specimens are calculated using (Eq. (4)), where the measured P-wave velocities are substituted for each sample. The impedance is calculated twice for each sample based on the velocities measured from both time point approaches as shown in Table 2. Both approaches present similar trends as to the P-wave velocity due to the linear relationship between the impedance and the velocity (Eq. (4)). Similarly, the variance in Z values is found less for the peak point approach compared to the arrival time

Table 2 Measured Mechanical Properties - Immersion Test Results

Specimen	V_l* (m/s)	V_l** (m/s)	$\boldsymbol{V_s}$* (m/s)	$\boldsymbol{V_s}$** (m/s)	Z* (kg/m^{2}s)	Z** (kg/m^{2}s)	E* (GPa)	E** (GPa)	G* (GPa)	G** (GPa)
Acr	2691	2685	1411	1425	3175380	3168300	0.872	0.872	0.128	0.128
Nyl	2403	2411	1094	1099	2762990	2772650	0.912	0.911	0.088	0.089
Cr_1	4672	4839	2602	2631	10511775	10887750	0.437	0.426	0.563	0.574
Cr_2	4620	4694	2551	2563	10395000	10561500	0.441	0.436	0.559	0.564
Cr_3	4617	4730	2467	2503	10388700	10642500	0.441	0.433	0.559	0.567
μ	4636	4754	2540	2566	10431825	10697250	0.440	0.431	0.560	0.569
σ	25	62	56	52	56592	138703	0.002	0.004	0.002	0.004
CV	0.5%	1.3%	2.2%	2.0%	0.5%	1.3%	0.4%	1.0%	0.3%	0.7%
Mr0%_1	4336	3650	2495	2438	9756900	8212500	0.462	0.522	0.538	0.478
Mr0%_2	4306	3911	2489	2469	9687600	8799750	0.464	0.498	0.536	0.502
Mr0%_3	4305	4190	2482	2490	9686250	9427500	0.464	0.474	0.536	0.526
μ	4316	3917	2489	2466	9710250	8813250	0.464	0.498	0.536	0.502
σ	15	220	5	21	32991	496114	0.001	0.020	0.001	0.020
CV	0.3%	5.6%	0.2%	0.9%	0.3%	5.6%	0.2%	4.0%	0.2%	4.0%
Mr15%_1	4477	4329	2568	2509	10073700	9740250	0.451	0.463	0.549	0.537
Mr15%_2	4420	4430	2476	2496	9944550	9967500	0.456	0.455	0.544	0.545
Mr15%_3	4305	4209	2412	2426	9686250	9470250	0.464	0.472	0.536	0.528
μ	4401	4323	2485	2477	9901500	9726000	0.457	0.463	0.543	0.537
σ	72	90	64	36	161078	203251	0.006	0.007	0.006	0.007
CV	1.6%	2.1%	2.6%	1.5%	1.6%	2.1%	1.2%	1.5%	1.0%	1.3%
Mr35%_1	4565	4560	2597	2539	10271250	10260000	0.445	0.445	0.555	0.555
Mr35%_2	4496	4560	2546	2496	10116000	10260000	0.450	0.445	0.550	0.555
Mr35%_3	4412	4538	2528	2544	9926550	10210500	0.456	0.447	0.544	0.553
μ	4491	4553	2557	2526	10104600	10243500	0.450	0.446	0.550	0.554
σ	63	10	29	22	140954	23335	0.005	0.001	0.005	0.001
CV	1.4%	0.2%	1.1%	0.9%	1.4%	0.2%	1.0%	0.2%	0.8%	0.1%
Mr50%_1	4777	4857	2768	2513	10748250	10928250	0.430	0.425	0.570	0.575
Mr50%_2	4707	4765	2716	2725	10590300	10721250	0.435	0.431	0.565	0.569
Mr50%_3	4697	4726	2365	2352	10568250	10633500	0.435	0.433	0.565	0.567
μ	4727	4783	2616	2530	10635600	10761000	0.433	0.430	0.567	0.570
σ	36	55	179	153	80163	123570	0.002	0.004	0.002	0.004
CV	0.8%	1.1%	6.8%	6.0%	0.8%	1.1%	0.6%	0.9%	0.4%	0.7%

*Based on peak point, **Based on arrival point

approach, measured with the coefficients of variance (*CV*) ranging between 0.3% and 1.6%; and 0.2% and 5.6%, respectively. The overall Z results indicate that the mortar has the least impedance while the concrete having the highest, which agree with the fact that the impedance increases as the material stiffness does due to the higher volumes of the larger particles in them. The influence

of additional stiffness due to the glass beads on the impedance is also examined with the plots given in Fig. 9. The figure displays the correlation between the impedance, mean impedance of the same class of mortar specimens, and the glass beads percent. For both reference point approaches, the Z curves demonstrate a linearly increasing trend with an increase in glass bead percent with the coefficients of determination (R^2) higher than 0.91.

The determination of acoustic impedances of water and specimens allows calculation of the coefficients of transmission (T_c) and reflection (R_c) at the interface of water and specimen. Fig. 10 presents both of the coefficients calculated by substituting the impedances derived from the arrival time and peak point approaches into (Eqs. (5) and (6)). The coefficients reveal the influence of the amount of larger grains over the ratio of the transmitted and reflected waves at the specimen-water interface. Compared to the cementitious samples, acrylic and nylon samples display a very high ratio of transmitted wave energy. Whereas the transmission coefficient reduces significantly to below 0.5 for the cement-based specimens meaning more than half of the wave energy is reflected. The transmission coefficients attained from four mortar specimens, which include different levels of glass beads from 0% to 50%, confirm that a higher amount of larger grains causes less transmitted wave energy and a higher reflected one. Regarding the concrete samples (Cr), on the other hand, the coefficients are found to be very close to the ones obtained from the mortar with 50% glass beads (Mr50%), despite these two types of material have two major differences. Firstly, the aggregate size in Cr is twice the glass bead in Mr50%; secondly, the uniformity of glass beads is much greater than the aggregates which means higher specific surface. Based on these findings, the influence of the aggregate size and shape on the acoustic parameters could not be observed, rather the stiffness increased due to the larger amount of aggregate/glass bead is believed to determine the transmitted/reflected wave ratio. Yet, derivation of the acoustic parameters described herein provides additional information on the material conditions, which can be conveniently obtained from the immersion test as it is difficult to attain them from the conventional UPV test.

4.1.3 Materials elastic moduli

The elastic moduli of the tested specimens, namely the Young's modulus (E) and shear modulus (G), are calculated using (Eqs. (9) and (10)) by substituting the P-wave and S-wave velocities obtained from the immersion tests, are given in Table 2. Like the wave parameters presented above, both moduli are derived from the velocities measured by both the first arrival and the peak point approaches. Since the Young's modulus is inherently related to the P-wave and S-wave velocities through the Poisson's ratio (Eq. (8)), and the shear modulus is related to the S-wave velocity (Eq. (10)), trends similar to those depicted in Fig. 8 are observed, as displayed in Fig. 11. Consequently, the variability observed earlier for P-wave velocity values obtained from both reference approaches is reflected in the Young's modulus for the same two mortar samples. Similarly, the S-wave velocity influences the shear modulus, as depicted in Fig. 11. The influence of the glass beads on the elastic properties of the mortar samples is also evident in the plots shown in Fig. 12. Both the mean Young's and shear moduli of the same class of mortar specimens exhibit a linear increase with respect to the percentage of glass bead, attributed to the additional stiffness they impart. Both reference point approaches yield a R^2 value higher than 0.9, indicating no significant drawback in using the peak point as the reference arrival time.

4.1.4 Attenuation coefficient

Wave attenuation is a critical material property that can provide valuable insight into the condition of concrete materials. The elastic material properties examined so far are related to the

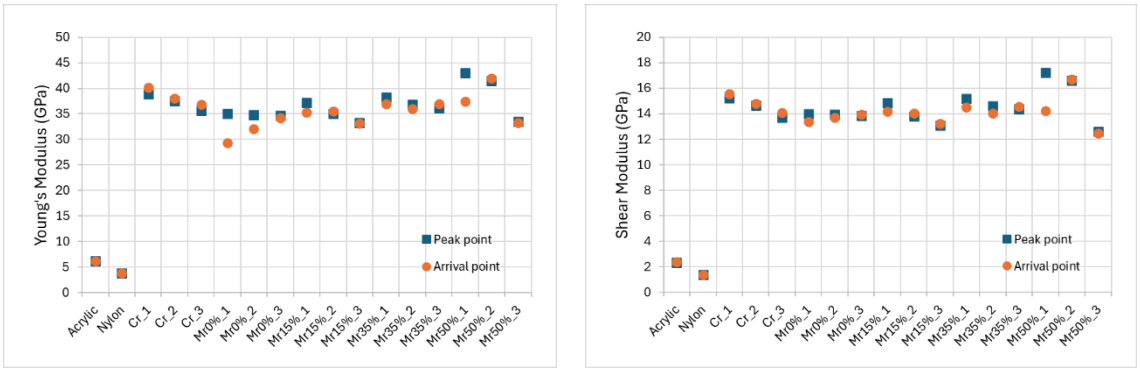

(a) P-wave velocity (b) S-wave velocity

Fig. 11 (a) Young's modulus and (b) shear modulus determined by two reference time point approaches, namely peak point and arrival point

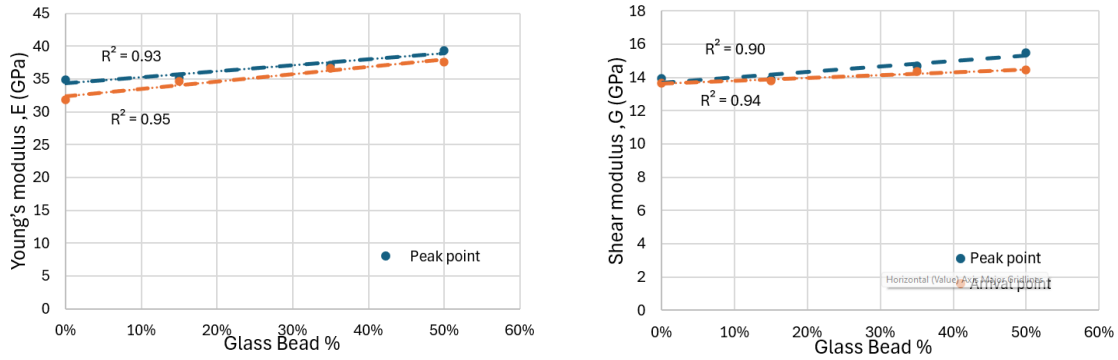

(a) P-wave velocity (b) S-wave velocity

Fig. 12 (a) Mean Young's modulus and (b) mean shear modulus with respect to glass bead %

material stiffness and density, the material attenuation can provide additional information regarding material heterogeneity. Herein, the attenuation coefficient for each test sample is determined by analyzing the peak amplitude in time domain (Peak_A) and the spectral area of the frequency spectrum (SA) of the waves recorded during the immersion measurements. Since the coupling in the water tank is constant and identical transducers are used for all samples, the measured decay in signal amplitudes or magnitudes should be solely attributed to material attenuation. This includes both absorption and scattering mechanisms which account for most of the total attenuation.

Table 3 presents the attenuation coefficients calculated based on two signal parameters, Peak_A and SA, using the method described in (Eq. (16)) for each specimen. The smallest attenuation coefficients are observed for the acrylic and nylon specimens as expected due to their homogenous structures, whereas an increase in grain size causes higher wave attenuation in the cementitious specimens, having the mortar and concrete specimens as the most attenuative materials. However, the added glass beads slightly reduce the attenuative behavior of mortar as illustrated in Fig. 13. The trends presented in the Fig. represent the variation in attenuation coefficient with respect to

Table 3 Attenuation coefficients from the immersion and LV tests

Material	Specimen Thickness	Attenuation coefficient (dB/mm) Immersion (Peak_A)	Immersion (SA)	Laser (Peak_A)	Laser (SA)
Acrylic		0.43	0.19	0.20	0.10
Nylon		038	0.17	0.19	0.12
Concrete	20 mm	1.68	0.78	0.58	0.53
	40 mm	1.10	0.52	0.33	0.32
	80 mm	0.61	0.33	0.21	0.17
Mortar	20 mm	1.58	0.74	0.50	0.44
	40 mm	1.11	0.52	0.29	0.29
	80 mm	0.88	0.44	0.20	0.20
Mortar+15%gb	20 mm	1.42	0.67	0.47	0.40
	40 mm	0.86	0.40	0.35	0.33
	80 mm	0.57	0.29	0.23	0.20
Mortar+35%gb	20 mm	1.05	0.48	0.40	0.34
	40 mm	0.84	0.40	0.28	0.27
	80 mm	0.61	0.30	0.20	0.18
Mortar+50%gb	20 mm	1.13	0.51	0.40	0.32
	40 mm	0.86	0.40	0.28	0.24
	80 mm	0.60	0.29	0.14	0.15

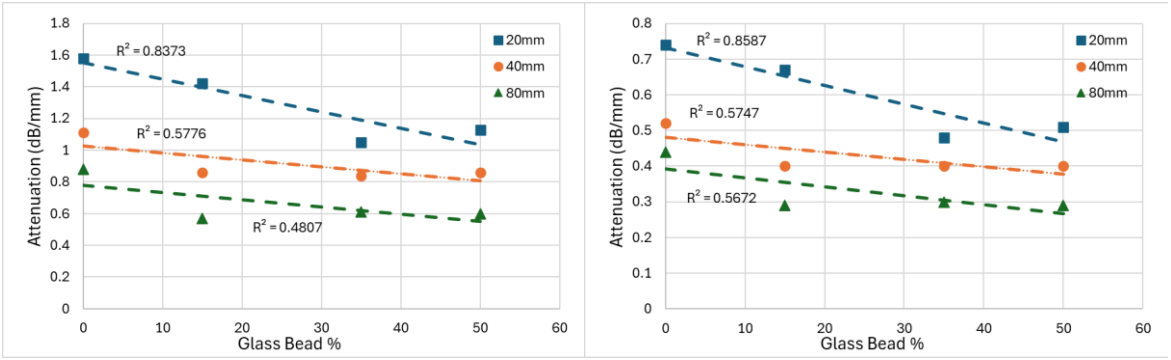

(a) P-wave velocity (b) S-wave velocity

Fig. 13 Attenuation coefficients from the immersion tests based on (a) Peak Amplitude, (b) Spectral Area

the amount of glass beads. The coefficients are grouped by the specimen thickness to eliminate the effect of the sample dimension on attenuation and expose the influence of heterogeneity caused by glass beads. Although, the plots shown in Fig. 13 do not demonstrate a significant correlation between the attenuation and the glass bead percent, with low values of R^2, a subtle but consistent decreasing trend in attention is observable for all three sets of specimens. Nevertheless, overall, all

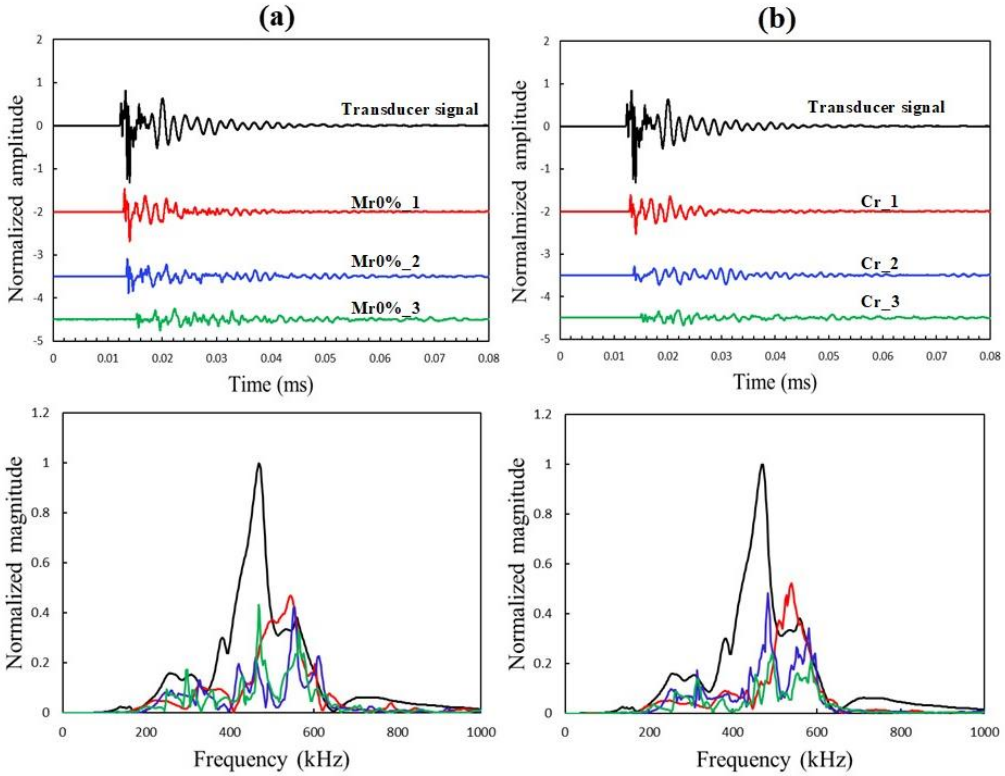

Fig. 14 Time histories and corresponding Fourier spectra for (a) mortar and (b) concrete

mortar specimens with glass beads exhibit less wave attenuation compared to regular mortar and concrete samples. This can be attributed to the higher acoustic impedance of glass beads (around 14.5 MRayls) compared to aggregate thereby allowing more incident wave pressure to be reflected at the surfaces of glass beads and subsequently reach the opposite side of the specimen. On the other hand, regarding the concrete specimens, it is observed that the attenuation coefficient is mostly higher compared to the same size of mortar counterparts. Given the fact that the measured Young's moduli are in the same order for the concrete (Cr) and the stiffer mortar (Mr 35% and Mr 50%) samples (Fig. 11), this high attenuative behavior of the concrete samples can be attributed to the irregular shape of the aggregates compared to the smooth surface of the glass beads. Lastly, calculating the attenuation coefficient using both signal parameters, peak amplitude and spectral area, provides close R^2 values, as shown in the plots in Fig. 13, with no noticeable improvement.

4.2 Laser test results

Laser vibrometer (LV) provides a non-contact method to inspect a broad range of structures from a distance where accessibility is not possible. Herein, a LV is utilized to determine the P-wave velocity and the attenuation coefficient for the characterization of the cementitious specimens. During the LV tests, the waves generated on the surface of the specimens are recorded while the transmitter is attached at the other side as illustrated in Fig. 4. Additionally, a reference

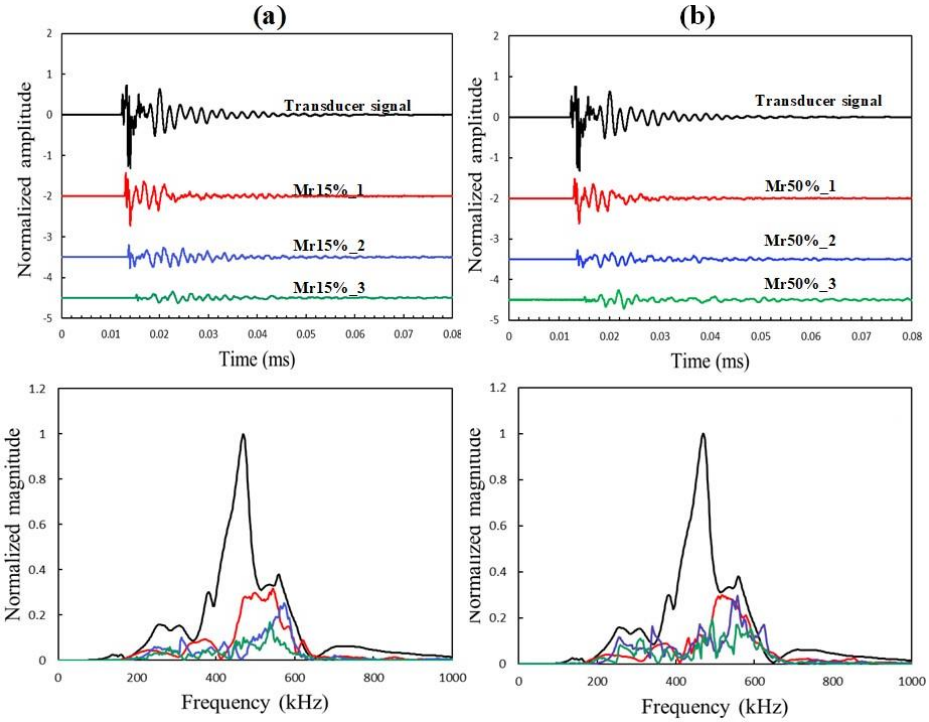

Fig. 15 Time histories and corresponding Fourier spectra for (a) Mr15% and (b) Mr50%

(transducer) signal is acquired at the bare transducer surface. The typical signals recorded on the mortar and concrete specimens are shown in Fig. 14. As similar to the immersion measurements, the laser reading indicates higher wave attenuation for the thicker specimens. Compared to the mortar specimens, the presence of coarse aggregates in concrete specimens promotes further attenuation. The frequency spectra for all the specimens reveal multiple peaks in the frequency domain in comparison to the spectra obtained from the immersion test, where only one signal peak exists. This is due to the fact that the water in the immersion tank allows only the P-wave mode to propagate filtering out all the other modes, whereas the signals measured by the LV contains all the components of the wave modes. Similar observations can also be done for the wave signals recorded on the mortars containing 15% and 50% glass beads as shown in Fig. 15. The signals measured during the LV tests are analyzed to determine two wave properties, the P-wave velocity and the attenuation coefficient. These two are then compared with the ones obtained from the immersion tests in order to explore the possibility of substituting two testing techniques with each other.

4.2.1 Wave velocity

The P-wave velocity is calculated by dividing the specimen thickness by the arrival time measured during the LV tests. The arrival time is determined as the time delay between the signal form the reference transducer and the wave signal acquired on the specimen's top surface. In Fig. 16, the P-wave velocities obtained from laser and immersion (peak point approach) measurements are presented together for comparison. The velocities from both tests exhibit consistent results.

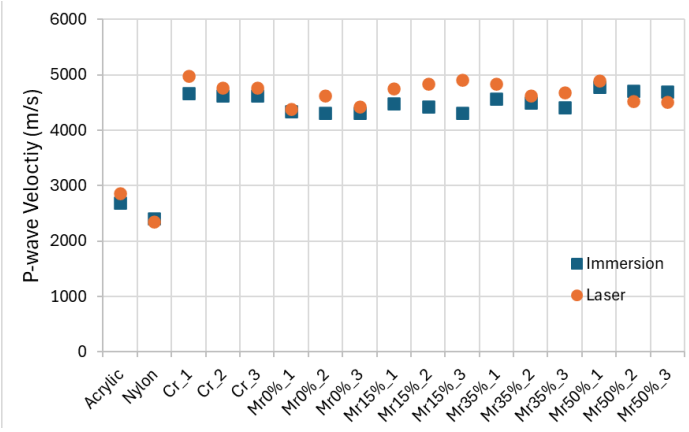

Fig. 16 The P-wave velocities obtained from the immersion (peak point approach) and laser tests

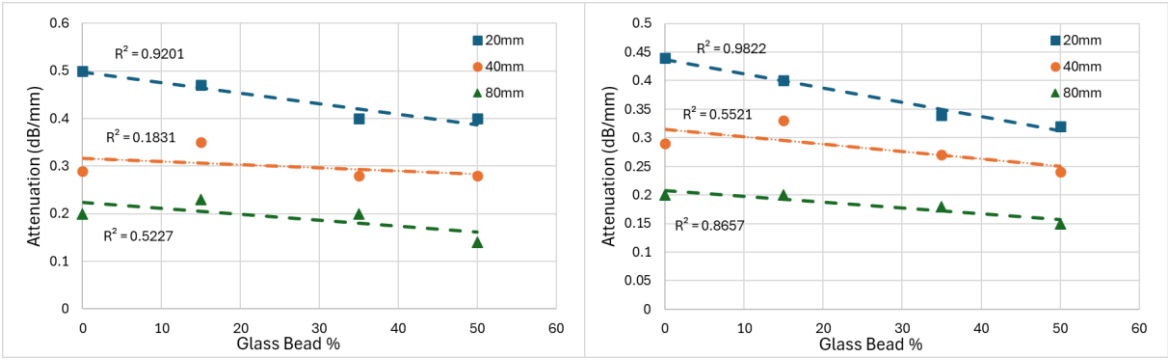

(a) P-wave velocity (b) S-wave velocity

Fig. 17 Attenuation coefficients from the LV tests based on (a) Peak amplitude and (b) Spectral area

Assuming the immersion tests provide the accurate P-wave velocities due to elimination of the other wave modes in the water, such as shear waves, the percent errors for all specimens range from 1% to 14%, with an average of 5%. This suggests that the LV test can serve as a viable alternative to immersion testing with an anticipated percent error in the order of 5%. However, it should be noted that, while the measured velocities are of the same order for both test methods, identifying the arrival time is more straightforward with the signals obtained from the immersion test. In contrast, the signals acquired using the LV method are noisier, requiring careful attention to detect the arrival time.

4.2.2 Attenuation coefficient

The attenuation coefficient is extracted from the signals measured with the LV in order to compare against the results obtained from the immersion tests. Similar to the immersion tests, the attenuation coefficient is calculated using (Eq. (16)) based on the same signal parameters, Peak_A and SA. The coefficients calculated based on these two parameters for both tests are given in Table 3. The table indicates similar findings for both tests, where the cementitious materials exhibit

higher attenuation due to their inherent heterogeneity with respect to the homogeneous reference specimens, acrylic and nylon. Consistent with the immersion test results, a reduced attenuation is measured for the mortars containing glass beads compared to the pure mortar as displayed with the trends depicted in Fig. 17. Despite relatively low R^2 values, these decreasing trends in attenuation with added glass beads are consistent across all specimen groups of the same dimensions and are also in agreement with the trends observed in the immersion tests (Fig. 13). An interesting observation, unlike the immersion tests results, utilizing spectral area (SA) as the signal parameter significantly improves the reliability of the attenuation trends. Comparing trends in Fig. 17, the R^2 values of the attenuation trends obtained with SA significantly surpass those derived from peak amplitudes in measured signals.

Another observation is that the attenuation coefficients obtained from the LV are smaller compared to those measured using the immersion tests for all the specimens tested. This is because, in the immersion tank, water acts as a filter, smoothing the signal and reducing the overall signal energy. In contrast, the air-coupled LV-based measurement captures the total signal energy, resulting in smaller attenuation values. Nevertheless, it should be noted that, unlike velocity measurement, attenuation measurement is not free from the influences of test setup, configuration, and specimen size. Therefore, a reference measurement is essential for interpreting attenuation behavior. However, in this study, since specimens with identical dimensions are compared to investigate the effect of aggregate size on attenuation, the comparative approach remains valid.

5. Conclusions

This study presents the results obtained from two different NDT tests, immersion through transmission and laser vibrometer, conducted to examine the effect of the grain size on the physical properties for cementitious materials. Two groups of specimens are tested: homogenous (acrylic and nylon) and heterogeneous (concrete and mortar with 0%, 15%, 35%, and 50% glass beads). Material characterization is performed based on multiple material properties, including P-wave and S-wave velocities, acoustic properties, elastic moduli, and attenuation coefficient. Furthermore, various signal parameters in both time and frequency domains are investigated to determine these material properties. The following conclusions are derived from the research findings:

- The peak point in a wave signal's time history can conveniently substitute the arrival time point for determining both P-wave and S-wave velocities.
- Both P-wave and S-wave velocities increase as the amount of the larger grain size in the mortar increases. Due to the inherit relationship between the wave velocities and the elastic properties, the Young's and shear moduli are also positively correlated with grain size.
- A higher amount of larger grains, represented by glass beads, in mortar leads to higher acoustic impedance and coefficient of reflection, and causes the coefficient of transmission to decrease because of the higher impedance of the larger grains.
- The concrete specimens mostly exhibit a higher attenuation coefficient compared to the mortars. Since other elastic properties are measured at the same order for the concrete and the stiffer mortar samples, this high attenuative behavior of concrete can be attributed to the irregular shape of aggregates compared to the smooth surface of glass beads.
- Overall, for determination of the material properties from the immersion tests, preferring the peak point, which can be conveniently identified on a recorded wave signal, as the reference

point instead of the arrival point improves the practicability of the velocity calculations without compromising accuracy.

- Specimen thickness is found to have minimal effect on the measured mechanical properties, with *CV*s ranging from 0.2% to 6.8%, indicating that the elastic properties can be used as an absolute measure for material characterization, whereas the attenuation coefficient is highly influenced by specimen size and should be interpreted in a relative manner.
- The LV tests provide P-wave velocity measurements with a percent error at an order of 5% with respect to the immersion tests.
- While both test methods yield consistent velocities, detecting the arrival time requires careful attention for the signals obtained from the LV due to their inherently noisier characteristics.
- LV-measured attenuation coefficients are based on the total signal energy, whereas immersion tests measure the attenuation of P-wave modes.
- Utilizing spectral area (SA) obtained from the LV tests for identifying material attenuation yields improved results compared to those from the immersion tests. Nevertheless, attenuation is highly influenced by the test setup and specimen size, so reference measurements are necessary for both methods.
- Based on these findings, it can be concluded that LV testing can serve as a viable alternative to immersion testing.

Acknowledgments

The authors would like to thank to Mustansiriyah University and the Natural Sciences and Engineering Research Council of Canada (NSERC) for their financial support for this research work.

References

ASTM C597-22 (2022), Standard Test Method for Pulse Velocity Through Concrete. ASTM International, West Conshohocken, PA.

ASTM C1383-23 (2023), Standard Test Method for Measuring the P-Wave Speed and the Thickness of Concrete Plates Using the Impact-Echo Method. ASTM International, West Conshohocken, PA.

Aggelis, D., Shiotani, T. and Polyzos, D. (2009), "Characterization of surface crack depth and repair evaluation using rayleigh waves", *Cement Concrete Compos.,* **31**(1), 77-83. https://doi.org/10.1016/j.cemconcomp.2008.09.008.

Anugonda, P., Wiehn, J.S. and Turner, J.A. (2001), "Diffusion of ultrasound in concrete", *Ultrasonics*, **39**, 429-435. https://doi.org/10.1016/S0041-624X(01)00077-4.

Bazylev, P.V. and Lugovoi, V.A. (2023), "Results of the COOMET 706/RU-A/16 pilot comparison of national standards of the unit of propagation velocity of longitudinal ultrasonic waves in solids", *Meas. Tech.*, **66**, 279-287. https://doi.org/10.1007/s11018-023-02222-9.

Becker, J., Jacobs, L.J. and Qu, J. (2003), "Characterization of cement-based materials using diffuse ultrasound", *J. Eng. Mech.*, **129**(12), 1478-1484. https://doi.org/10.1061/(ASCE)0733-9399(2003)129:12(1478),

Bilaniuk, N. and Wong, G.S. (1993), "Speed of sound in pure water as a function of temperature", *J. Acoust. Soc. Am.*, **93**(3), 1609-1612. https://doi.org/10.1121/1.406819.

Buiochi, F., Andrade, M.A.B., Pérez, N. and Adamowski, J.C. (2014), "Ultrasonic Characterization of

Anisotropic Materials", *Comprehensive Materials Processing*, Elsevier, Amsterdam, **2**, 65-81.
Chaix, J.F., V. Garnier, V. and Corneloup, G. (2006), "Ultrasonic wave propagation in heterogeneous solid media: theoretical analysis and experimental validation", *Ultrasonics*, **44**(2), 200-210. https://doi.org/10.1016/j.ultras.2005.11.002.
Ensminger, D. and Bond, L.J. (2011), *Ultrasonics: Fundamentals, Technologies, and Applications*, (3rd Ed.), CRC Press. https://doi.org/10.1201/b11173.
Gaydecki, P., Burdekin, F., Damaj, W. and John, D. (1992), "The propagation and attenuation of medium-frequency ultrasonic waves in concrete: A signal analytical approach", *Meas. Sci. Technol.*, **3**(1), 126. https://doi.org/10.1088/0957-0233/3/1/018.
Ginzel, E. and Turnbull, B. (2016), "Determining approximate acoustic properties of materials", *e-J. Nondestruct. Test.* https://www.ndt.net/?id=20452.
Gosálbez, J., Wright, W.M.D., Jiang, W., Carrión, A., Genovés, V. and Bosch, I. (2018), "Airborne non-contact and contact broadband ultrasounds for frequency attenuation profile estimation of cementitious materials", *Ultrasonics*, **88**, 148-156.
Gucunski, N., Kee, S.H., La, H., Basil, B. and Maher, A. (2015), "Delamination and concrete quality assessment of concrete bridge decks using a fully autonomous RABIT platform", *Struct. Monit. Maint.*, **2**(1), 19-34. https://doi.org/10.12989/smm.2015.2.1.019.
Hasannejad, M., Berenjian, J., Pouraminian, M. and Sadeghi Larijani, A. (2022), "Studying of microstructure, interface transition zone and ultrasonic wave velocity of high strength concrete by different aggregates", *J. Build. Pathology \Rehab.*, **7**(9). https://doi.org/10.1007/s41024-021-00146-x.
Hellier, C. (2001), *Handbook of Nondestructive Evaluation*, McGraw-Hill, New York, United States.
Ju, J.W., Weng, L. and Liu, Y. (1999), "Effects of exciting fFrequency and grain size in ultrasonic NDE of concrete", *Proceedings of the ASME 1999 International Mechanical Engineering Congress and Exposition on the Recent Advances of the Ultrasonic Nondestructive Evaluation and Composite Material Characterization*, Nashville, Tennessee, USA, November. https://doi.org/10.1115/IMECE1999-0885.
Kirlangic, A.S., Cascante, C. and Polak, M.A. (2016), "Assessment of concrete beams with irregular defects using surface waves", *ACI Mater.*, **113**(1), 73-81.
Kirlangic, A.S., Cascante, G. and Salsali, H. (2020), "New diagnostic index based on surface waves: Feasibility study on concrete digester tank", *J. Perform. Constr. Fac.*, **34**(6). https://doi.org/10.1061/(ASCE)CF.1943-5509.0001522.
Kirlangic, A.S. and Iscan, Z. (2022), "Estimation of crack depth in steel-fiber reinforced concrete using ultrasonic surface waves", *Struct. Monit. Maint.*, **9**(4), 373-388. https://doi.org/10.12989/smm.2022.9.4.373.
Kim, Y.H., Lee, S. and Kim, H.C. (1991), "Attenuation and dispersion of elastic waves in multi-phase materials", *J. Phys. D: Appl. Phys.*, **24**(10), 1722. https://doi.org/10.1088/0022-3727/24/10/005.
Krautkrämer, J. and Krautkrämer, H. (2013), *Ultrasonic testing of materials*, (3rd Ed.), Springer Science and Business Media.
Lin, S., Shams, S., Choi, H., Meng, D. and Azari, H. (2020), "Estimation of wave velocity for ultrasonic imaging of concrete structures based on dispersion analysis", *ASTM Int. J. Test. Eval.*, **48**(2), 1095-1107. https://doi.org/10.1520/JTE20180343.
O'Leary, R.L., Hayward, G., Smillie, G. and Parr, A. (2002), CUE Materials Database, Technical Report, Centre for Ultrasonic Engineering, University of Strathclyde, Glasgow, Scotland
Otsuki, N., Iwanami, M., Miyazato, S. and Hara, N. (2000), "Influence of aggregates on ultrasonic elastic wave propagation in concrete", *Nondestruct. Test. Civil Eng.*, 313-322.
Webster, J.G. and Eren, H. (2014), *Measurement, Instrumentation, and Sensors Handbook: Spatial, Mechanical, Thermal, and Radiation Measurement*, (2nd Ed.), CRC Press. https://doi.org/10.1201/b15474.
Pham, Q.Q., Dang, N.L. and Kim, J.T. (2021), "Piezoelectric sensor-embedded smart rock for damage monitoring in a prestressed anchorage zone", *Sensors*, **21**(2), 353. https://doi.org/10.3390/s21020353.
Philippidis, T.P. and Aggelis, D.G. (2005), "Experimental study of wave dispersion and attenuation in concrete", *Ultrasonics*, **43**(7), 584-595. https://doi.org/10.1016/j.ultras.2004.12.001.
Polytec GmbH. (2013), *User manual: Fiber-coupled vibrometer sensor head OFV-534*. Waldbronn,

Germany.
Punurai, W. (2006), "Cement-based materials' characterization using ultrasonic attenuation", Ph.D. Dissertation, Georgia Institute of Technology.
Selfridge, A.R. (1985), "Approximate material properties in isotropic materials", *IEEE T. Sonic. Ultrason.*, **32**(3), 381-394.
Shiotani, T., Ogura, N., Okude, N., Watabe, K., Van Steen, C., Tsangouri, E., Lacidogna, G., Czarnecki, S., Chai, H.K., Yang, Y., Verstrynge, E. and Aggelis, D. (2024), "Non-destructive inspection technologies for repair assessment in materials and structures", *Develop. Built Environ.*, **18**, 100443. https://doi.org/10.1016/j.dibe.2024.100443.
Ta, Q.B., Pham, Q.Q., Pham, N.L., Huynh, T.C. and Kim, J.T. (2024), "Smart aggregate-based concrete stress monitoring via 1D CNN deep learning of raw impedance signals", *Struct. Control Health Monit.,* https://doi.org/10.1155/2024/5822653.

JK